Oxidative Degradation of Benzene in the Troposphere. Theoretical Mechanistic Study of the Formation of Unsaturated Dialdehydes and Dialdehyde Epoxides

Federica Motta, Giovanni Ghigo, and Glauco Tonachini*

Dipartimento di Chimica Generale ed Organica Applicata, Università di Torino, Corso Massimo D'Azeglio 48, I-10125 Torino, Italy

Received: December 21, 2001

Unsaturated dialdehydes and their epoxides are toxic products involved in aerosol formation and in the chemistry of the photochemical smog. They are detected when benzene is oxidatively degradated in the troposphere or in experiments that simulate tropospheric conditions. This theoretical study is focused at assessing the viability of some benzene oxidation channels that lead to their formation and could either follow or flank the previously studied pathway to hexa-2,4-diene-1,6-dial (muconaldehyde). In the former case, further oxidative degradation of muconaldehyde entails NO intervention and easily leads to glyoxal and butenedial, as secondary oxidation products. In the latter case, the pathways examined branch from an early intermediate in benzene oxidation, the 2-hydroxy-cyclohexadienyl peroxyl radical, and originate either from the corresponding oxyl radical **VI** (the "channel VI") or from the bicyclic endo-peroxy allyl-radical intermediate **XIII**, generated by the closure of a peroxy bridge (the "channel XIII"). The channel XIII can produce epoxy muconaldehyde without NO involvement, as well as some epoxy butenedial, glyoxal, and butenedial, as minor products and through NO-mediated pathways. Though the epoxy aldehydes could also form from the radical **VI**, through NO-mediated pathways, this is not competitive with the formation of muconaldehyde from **VI**. How a variable NO concentration can modulate the relative importance of the channel XIII vs the channel VI is estimated. Other pathways have been investigated and discarded as less favorable.

Introduction

Benzene, its methylated derivatives, and other aromatics contribute significantly to the atmospheric pollution, especially in urban areas, and can be of serious concern to the human health.[1−4] Their tropospheric oxidation processes produce a variety of compounds that have been only partially identified.[4] Benzene oxidation is believed to begin with the addition of the reactive hydroxyl radical to the aromatic ring. The initial intermediate is thus the hydroxy-cyclohexadienyl radical **I**. From this species, several reaction pathways can originate. Though a significant amount of data has been collected so far, the mechanistic details of the reaction steps leading to further oxidation of **I** need to be revealed through the hopefully synergic concourse of additional experimental and theoretical studies.

The oxidative pathways can be characterized by monomolecular steps or by the involvement of other species, as O_2, $HO^{\bullet}$, or NO. These have different reactivities,[5] and their concentrations are variable:[2,4,6] from the ca. 10^6 molecules cm^{-3} of hydroxyl, through the range of values encountered for the nitrogen oxides, typically 10^8-10^9 molecules cm^{-3}, up to the relatively high concentration of dioxygen, ca. 10^{18} molecules cm^{-3}. Different environmental conditions can thus in principle modulate the relative importance of possibly competing pathways. Of particular importance seems to be the concentration of nitrogen oxides (NO and NO_2) that shows peaks of even 10^{12} molecules cm^{-3} in very polluted areas[6] and is usually reported as a collective NO_x concentration.

Among the products identified in different experiments on the oxidation of benzene and methylated benzenes, we could mention phenols;[8] 1,2-, 1,4-, and 1,6-unsaturated dicarbonyls[9−12] (compare also ref 1 pp 374 and 375); epoxy and hydroxy derivatives of dicarbonyl compounds;[11] as well as furan derivatives[13] and other ring compounds as maleic anhydride.[14] Among the oxidation products, the aldehydes are important because (apart from exhibiting some toxicity on their own) they are involved in aerosol formation and take part in the chemistry of the photochemical smog.[6] This occurs through their transformation into peroxyacyl nitrates, $R.CO.OONO_2$, known to be irritating agents for the eyes and phytotoxic. In the case of benzene, the dicarbonyls detected are glyoxal **XX**, butenedial **XXI**, and muconaldehyde **VIII** (hexa-2,4-diene-1,6-dial; Chart 1**)**. The first two could form both by direct oxidation of this 1,6-dicarbonyl precursor or through independent ring fragmentation reactions distinct from those producing muconaldehyde.

The fact that the details of the oxidative degradation following the formation of **I** are not completely known[3] and that even the nature of many oxidation products is not determined[4,14] encourages us to pursue theoretical investigations, as has been done very recently also by other researchers on different systems.[15] Useful mechanistic and thermochemical information are expected, which will be complementary to the mass of experimental results accumulated as yet.

Our foregoing theoretical studies on the oxidative degradation of benzene were intended as such a contribution. The first study[16] dealt with three different attacks of O_2 on **I** and indicated that both irreversible phenol formation, through abstraction by O_2 of the H *gem* to OH in **I (**Chart 1**)**, and reversible O_2 addition

* To whom correspondence should be addressed. E-mail: glauco.tonachini@unito.it. Fax: 39-011-6707642.

10.1021/jp015619h CCC: $22.00
Published on Web 04/06/2002

CHART 1

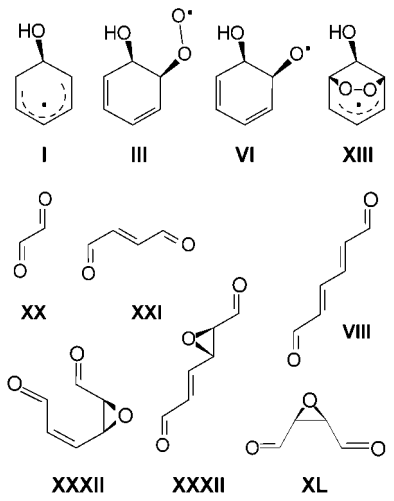

(yielding the 2-hydroxycyclohexadienyl peroxyl radical intermediate **III**) were realistic initial phases of benzene degradation. In the second study,[17] the subsequent steps which lead to the formation of the carcinogenic, cytotoxic, and genotoxic[18,19] muconaldehyde **VIII** were studied. A viable pathway, evolving through the NO-mediated formation of the oxyl radical **VI** from the peroxyl radical **III**, and its β-fragmentation, was compared with an alternate monomolecular step that generates the [3.2.1] bicyclic endo-peroxy allyl radical intermediate **XIII** by ring closure of **III** (see Figure 5 of ref 17).

In addition, some theoretical investigations on the tropospheric oxidation of aromatics have been carried out in the last years by other research groups and can be mentioned here. There was a 1995 DFT study on toluene,[20] aimed to identify plausible O_2 addition intermediates. Also, there was a 1996 semiempirical UHF/PM3 study[21] of the intermediates in hydroxyl and dioxygen addition to four methylated hydroxy-cyclohexadienyl radicals (transition structures were located by an approximate procedure), followed by DFT(B3LYP) single-point energy calculations. Relevant thermochemical properties were calculated in 1996[22] by the same semiempirical approach, used in conjunction with thermochemical group additivity rules.[23] More recently, the hydroxyl attack on toluene was studied by MP2 and DFT-(B3LYP) optimizations, followed by MP4 and coupled cluster (CCSD) energy difference estimates.[24] Similarly to ref 20, the relative stability of several HO−toluene−O_2 isomeric adducts has been investigated by MP2 and DFT(B3LYP) calculations.[25]

The complex picture of the conceivable pathways branching from benzene is further explored in the present theoretical investigation,[26] with the purpose of ascertaining the most probable channels leading to glyoxal and butenedial, as well as to epoxidized derivatives of the unsaturated dialdehydes. Some of the reactions that lead to furan and furan derivatives have points of contact with those dealt with here and will be discussed in a forthcoming paper.

In some transformations, intramolecular steps may intervene, as well as reactions with the hydroxyl radical or H abstraction by dioxygen. These reactions can be reasonably postulated even in conditions of low pollution. By contrast, other processes involve dioxygen addition and consequently require the intervention of NO, which transforms peroxyl radicals into oxyl radicals, and thus may prompt β fragmentation. The importance of the latter reactions can rise in case of a relatively high nitrogen oxide concentration. Thus, in comparing the more likely gas-phase pathways, the different situations corresponding to high and low NO_x concentration have to be taken into account.

Some reaction pathways considered in this study originate either from **XIII** or from **VI**, whose direct common precursor is the peroxyl radical **III**, which is one of the very first intermediates in the benzene oxidation process (Chart 1). All structures displayed in Chart 1 and in the schemes that follow are numbered by bold roman numerals consistently with the ordering of the two preceding papers.[16,17] These pathways lead to glyoxal **XX** and butenedial **XXI** or to the epoxidized dialdehydes **XXXII** and **XL (**Chart 1**)**. The 1,4- and 1,2-dialdehydes can be generated through different channels. One possibility is the further oxidation of **VIII** (section 1). An alternative is offered by a NO-mediated pathway that originates from **XIII** (section 2). In addition, other pathways can branch from **VI** and **XIII** and then converge on an oxyl epoxy intermediate, **XXVI**, from which the epoxidized muconaldehyde **XXXII** is obtained (section 3). Another NO-mediated pathway heads off from the preceding one, in correspondence of **XXVI**, and leads to the epoxidized butenedial **XL** (section 4). How butenedial (and muconaldehyde) could directly transform into their epoxy derivatives is briefly examined in section 5. Finally, a third pathway leading to glyoxal and butenedial and starting from **VI** (but not involving **VIII**) has been considered (section 6). All of these possibilities are described in detail in the Results section.

Method

The study of the reaction pathways was performed by determining the critical points of the reaction energy hypersurfaces that correspond to stable and transition structures (TS). All structures were fully optimized using gradient procedures[27] at the DFT (B3LYP) level of theory,[28,29] with the polarized split-valence shell 6-31G(d) basis set.[30a] The more important optimum interatomic distances reported in the figures are in angstroms. The nature of the critical points optimized was checked by diagonalization of the 6-31G(d) analytic Hessian (vibrational analysis). Energies were refined by DFT(B3LYP)/6−311+G(d,p)//6-31G(d) single-point calculations.[30b,c] The doublet energies so computed were corrected for spin contamination by the quartet, by using a formula analogous to that suggested by Yamaguchi.[31,32] The corrected energies were used in turn, in conjunction with the above-mentioned vibrational analysis data, to evaluate the activation and reaction enthalpies and free energies.[33] ΔG values (and to some extent ΔH values) based on the relevant spin-projected 6-311+G(d,p) energies, will be discussed throughout the text. All calculations were carried out by using the Gaussian 98 system of programs.[34]

The oxidative degradation of muconaldehyde to glyoxal and butenedial was chosen at the outset as a benchmark to compare the results of 6-31G(d) optimizations with those obtained with a more extended basis set, denoted as 6-31(+)G(d), in which diffuse sp functions[30b] were added on the oxygen atoms. This basis set had been used in the geometry optimizations of two preceding studies.[16,17] The geometries of seven minima and three transition structures relevant to Scheme 1 (see the next section) were obtained with the two basis sets and resulted not to differ significantly. Then, DFT(B3LYP)/6-311+G(d,p)//6-31G(d) calculations were compared to DFT(B3LYP)/6-311+G(d,p)//6-31(+)G(d) calculations, and enthalpy and free energy differences were found to be at variance by 0.22 kcal mol^{-1} at most. Therefore, the procedure of using the 6-31G(d) optimized structures in the final single-

point calculations with the more extended 6−311+G(d,p) basis set was deemed safe and adopted throughout the study. A similar test was also carried out by adding p polarization functions on the hydrogens in the DFT(B3LYP)/6-31G(d,p) optimizations pertaining to a H-transfer process. DFT(B3LYP)/6-311+G(d,p) energy calculations on these geometries differ by only 0.02 kcal mol^{-1} from those carried out on the 6-31G(d) geometries. Details on both tests are in the Supplementary Information.

Results

The various reaction pathways mentioned in the Introduction will be described in detail presently. Enthalpy and free energy relative values are collected in Tables 1−5. In the text, every $\Delta G^{\ddagger}$ barrier and the ΔG for the related step will be reported by making reference to the foregoing energy minimum, and compared with the relevant enthalpy differences, when these differ significantly, to call attention to the entropy contribution. All free energy plots make reference to the closest closed-shell precursor molecule. So, in all free energy profiles but one, the reference zero line corresponds to benzene plus all small species involved in the steps shown in that figure. The exception is the plot in Figure 1a, in which the closed shell intermediate **VIII** is chosen as the reference instead of benzene.

1. Formation of Glyoxal and Butenedial from Muconaldehyde. In polluted areas, the significant concentration of nitrogen oxides opens a pathway leading to the 1,2- and 1,4-dialdehydes through the intervention of the NO radical on intermediates previously oxidized by hydroxyl and dioxygen.

A kinetic study of the reaction of hydroxyl with hexa-2,4-diene-1,6-dial **VIII** and 2-methylhexa-2,4-diene-1,6-dial has shown that these compounds react very promptly with HO• ($k \approx 1 \times 10^{-10}$ molecules^{-1} cm^3 s^{-1}).[37] Glyoxal, butenedial, and their methylated derivatives are the expected products of the hydroxyl-initiated oxidative degradation pathways.[10]

VIII can initially undergo complexation with hydroxyl and then addition to C^2 (Scheme 1). The rather small free energy barrier of 6 kcal mol^{-1} is accompanied by a negative ΔH estimate in correspondence of the TS, −2 kcal mol^{-1} (i.e., 1.5 above the complex). The adduct **XV** is then obtained with a large free energy drop with respect to the separate reactants, −27 kcal mol^{-1}, which corresponds to an even larger enthalpy difference, −37 kcal mol^{-1}. Addition to C^3 is not favored: the relevant adduct is ca. 13 kcal mol^{-1} higher in electronic energy than **XV**. Then, dioxygen addition to **XV** gives the peroxyl radical **XVI**, which is located ca. 8 kcal mol^{-1} above the two reactants, **XV** and O_2. The barrier for this endoergic step is 14 kcal mol^{-1} high. By contrast, in terms of enthalpy change, this step is exothermic by −2 kcal mol^{-1}, and the barrier is only 3 kcal mol^{-1} high. Reduction to the relevant oxyl radical is a necessary step toward the final β fragmentation. NO intervention accomplishes the task. (O_2 addition is more or less reversible in function of the NO concentration: though the free energy profile suggests a favored forward process toward the oxyl radical, low [NO] could cause the velocity of the backward process to be competitive.) First, a peroxynitrite adduct **XVII** is formed, without any free energy barrier. It is located almost 6 kcal mol^{-1} below the reactants **XVI** and NO. In terms of enthalpy, the step is more exoergic: −17 kcal mol^{-1}. Then, dissociation by cleavage of the O−O bond to the oxyl radical **XVIII** and NO_2 takes place. Although exiting the shallow dip on the enthalpy profile requires only 2 kcal mol^{-1}, in terms of ΔG, there is a further gain of −14 kcal mol^{-1}. If the backward process on the enthalpy profile is considered, no reassociation barrier is present for the separate fragments **XVIII** and NO_2 (to form the peroxinitrite **XVII** again). By contrast, the traits of the free energy reaction profile imply that the role as intermediate of the peroxynitrite adduct **XVII** is uncertain. A similar picture emerged in the preceding paper, concerning the formation of **VIII**.[17] A final β fragmentation of the oxyl radical produces s-cis (z for short) **XIX**, a radical precursor of glyoxal **XX**, and butenedial **XXI**. This step is very easy: both the enthalpy and free energy estimates of the barrier suggest that it is very low or even absent.

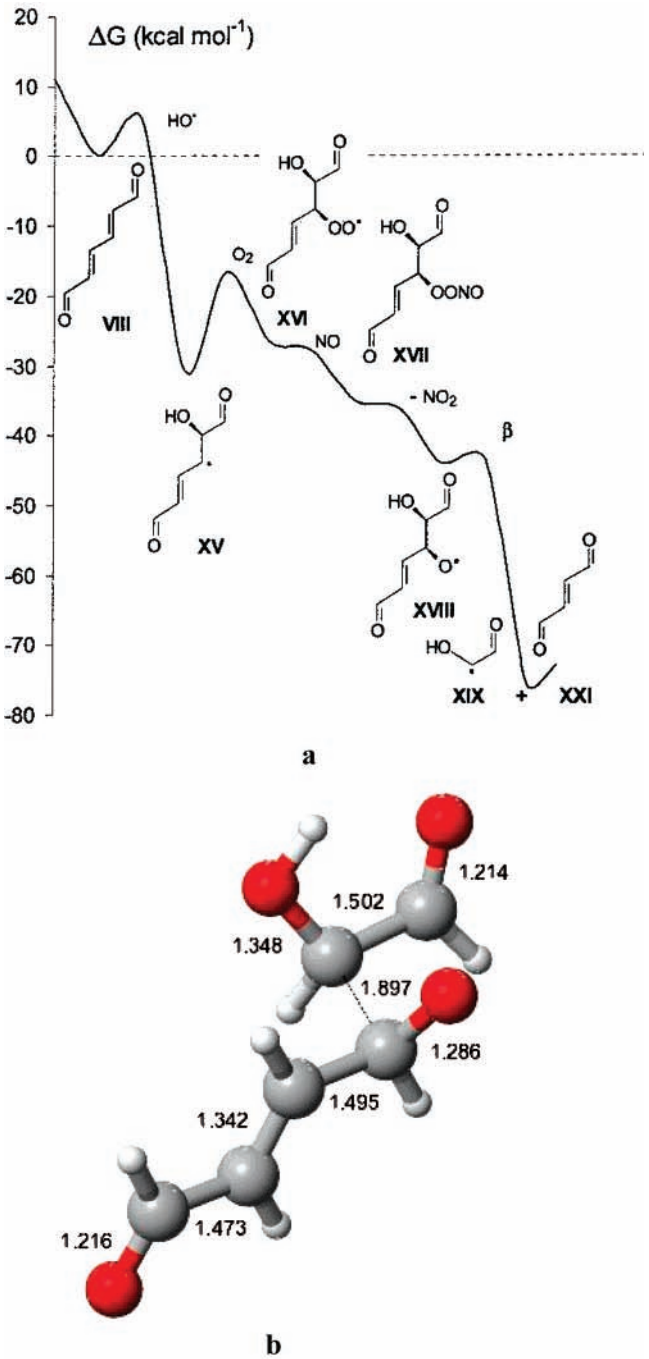

Figure 1. (a) Free energy profile for the formation of glyoxal and butenedial by oxidative degradation of muconaldehyde. (b) The β fragmentation transition structure (**XVIII** → **XIX** + **XXI**). Bond lengths are in Å, and angles are in degrees.

The free energy profile is shown in Figure 1a. In it, the reference "zero" line is set to the "**VIII** + HO• + O_2 + NO" limit. The β fragmentation transition structure (**XVIII** → z-**XIX**+**XXI**) is displayed in Figure 1b.

SCHEME 1

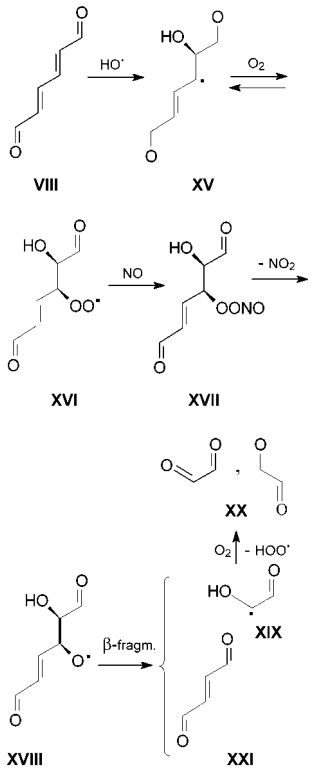

TABLE 1: Formation of Glyoxal and Butenedial from Muconaldehyde VIII[a]

	ΔE^b	ΔE^c	ΔH^d	ΔG^d
muconaldehyde **VIII** + HO•	0.0	0.0	0.0	0.0
VIII−OH complex	−9.6	−5.4	−3.8	4.6
TS **VIII** → **XV**	−3.9	−3.0	−2.3	6.3
XV	−43.6	−40.0	−37.4	−27.1
XV + O_2	0.0	0.0	0.0	0.0
TS **XV** → **XVI**	2.3	2.4	3.1	14.1
XVI	−8.9	−4.8	−2.4	8.4
XVI + NO	0.0	0.0	0.0	0.0
peroxynitrite **XVII**	−21.6	−18.7	−17.2	−5.8
XVIII + NO_2	−16.4	−18.4	−19.0	−19.9
XVIII	0.0	0.0	0.0	0.0
TS **XVIII** → z-**XIX** + **XXI**	1.4	0.7	−0.2	−0.1
z-**XIX** + butenedial **XXI**	−18.2	−21.2	−22.6	−34.7
z-**XIX** + O_2	0.0	0.0	0.0	0.0
H-abstraction TS z-**XIX** → z-**XX**	17.6	13.9	13.7	22.0
z-**XX** (glyoxal) + HOO•	10.8	10.5	9.4	7.6
TS z-**XIX** → z-**XIX**-O_2 adduct	1.6	0.7	1.2	11.0
z-**XIX**-O_2 adduct	−10.7	−7.4	−5.6	4.7
e-**XIX**-O_2 adduct	−9.2	−6.0	−8.1	2.6
TS e-**XIX**-O_2 → e-**XX** + HOO•	1.0	4.2	2.0	12.7
e-**XX** (glyoxal) + HOO•	6.6	6.0	5.0	3.4

[a] For each reaction step: energy, enthalpy, and free energy values (kcal mol^{-1}) relative to each preceding intermediate or intermediate plus reactant. Bold roman numerals make reference to Scheme 1. [b] From DFT(B3LYP)/6-31G(d) energy values obtained at the geometries optimized at the same level. [c] From DFT(B3LYP)/6-311+G(d,p) energy evaluations with correction of spin contamination (at the DFT(B3LYP)/6-31G(d) optimized geometries). [d] From enthalpy or free energy values estimated at 298.15 K. Differential zero-point energy corrections are computed at the DFT(B3LYP)/6-31G(d) level.

A final phase is needed to produce glyoxal. As a first possibility, H abstraction by O_2 in z-**XIX** can give directly z-glyoxal **XX**. This demands to get ahead of a barrier of 22 kcal mol^{-1}. z-Glyoxal and HOO• are higher in energy than the reactants by more than 7 kcal mol^{-1}. As an alternative, dioxygen can add to z-**XIX**, with a barrier of 11 kcal mol^{-1}, in a slightly endoergic step (less than 5 kcal mol^{-1}). The most stable isomer of the adduct is however the s-trans (e for short), which is less than 3 kcal mol^{-1} above the reactants. In an eliminative step from this e-adduct (with a barrier of 10 kcal mol^{-1}), HOO• forms again, together with e-glyoxal. These final products are somewhat higher than 3 kcal mol^{-1} with respect to the reactants. The situation is similar to that encountered in the formation of muconaldehyde (ref 17, Table 3, Figures 2 and 3).

SCHEME 2

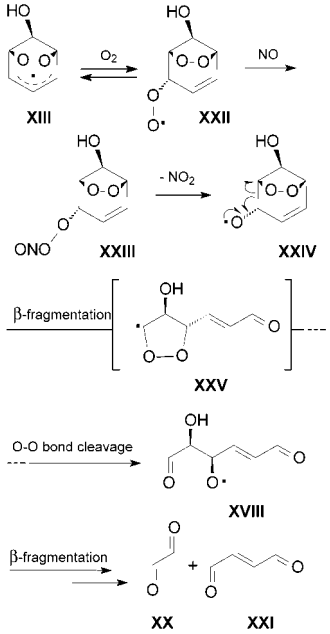

TABLE 2: Formation of Glyoxal and Butenedial from the [3.2.1] Bicyclic Endo-Peroxy Allyl Radical Intermediate XIII[a]

	ΔE^b	ΔE^c	ΔH^d	ΔG^d
XIII + O_2	0.0	0.0	0.0	0.0
TS **XIII** → **XXII**	1.1	0.3	1.0	10.8
XXII	−17.1	−13.2	−10.4	0.9
XXII + NO	0.0	0.0	0.0	0.0
peroxynitrite **XXIII**	−21.1	−17.8	−16.4	−4.7
XXIV + NO_2	−13.3	−15.3	−16.3	−17.4
XXIV	0.0	0.0	0.0	0.0
TS **XXIV** → **XVIII**	8.3	6.2	5.2	4.7
XVIII	−49.5	−55.5	−56.3	−60.8

[a] For each reaction step: energy, enthalpy, and free energy values (kcal mol^{-1}) relative to each preceding intermediate or intermediate plus reactant. Bold roman numerals make reference to Scheme 2. [b] From DFT(B3LYP)/6-31G(d) energy values obtained at the geometries optimized at the same level. [c] From DFT(B3LYP)/6-311+G(d,p) energy evaluations with correction of spin contamination (at the DFT(B3LYP)/6-31G(d) optimized geometries). [d] From enthalpy or free energy values estimated at 298.15 K. Differential zero-point energy corrections are computed at the DFT(B3LYP)/6-31G(d) level.

2. Glyoxal and Butenedial from the Bicyclic Early Intermediate XIII. Another path to the same dialdehydes can be followed by starting off back from the intermediate **XIII**. This species is the ring-closure derivative of the peroxyl radical **III**, which is one of the earlier oxidation products of benzene.[16] In the previously discussed pathway, the benzene ring had first to be opened to give **VIII**,[17] and then a further oxidation occurred (Scheme 1). In contrast, an additional oxidation of the original six-membered ring, still present in **XIII**, takes place in the processes discussed in this section, and ring opening occurs at a later stage (Scheme 2). To our knowledge, this pathway

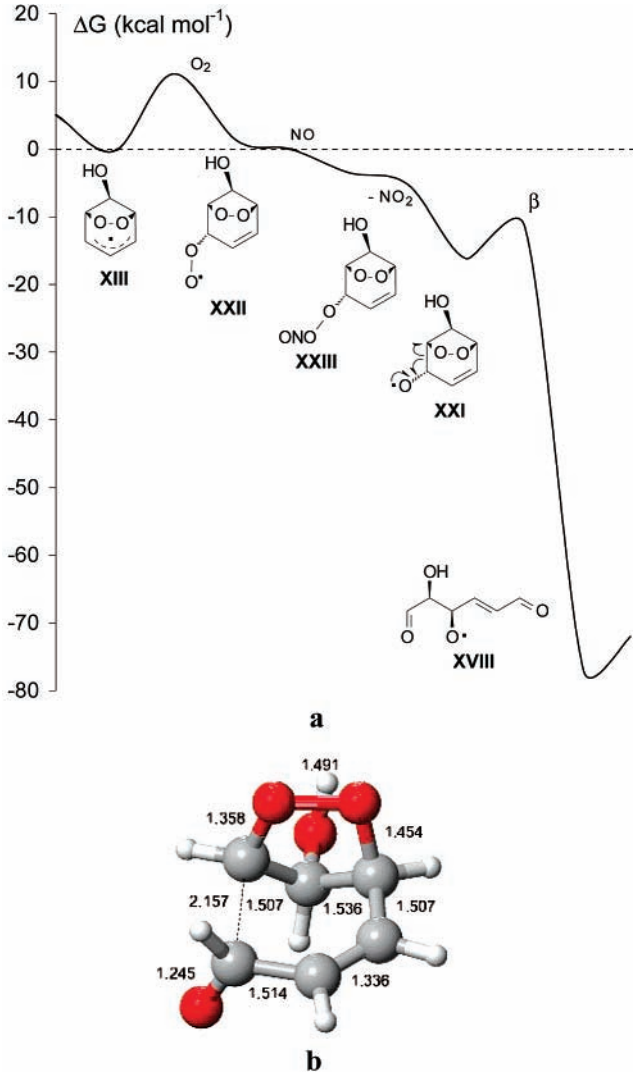

Figure 2. (a) Free energy profile for the formation of glyoxal and butenedial from the endoperoxy intermediate **XIII**. (b) The β fragmentation and O−O bond cleavage transition structure (**XXIII** → **XVIII**). Bond lengths are in Å, and angles are in degrees.

was first proposed by Darnall, Atkinson, and Pitts in 1979[38] and later on discussed by Yu, Jeffries, and Sexton.[10]

The endo-peroxy radical intermediate **XIII** can be attacked by dioxygen, thus producing the peroxyl radical **XXII**. This step (Scheme 2) requires the subsequent intervention of NO to transform the peroxyl group into oxyl. The peroxyl radical **XXII** is obtained with the free energy barrier estimate of 11 kcal mol^{-1}, in correspondence of the TS geometry. This reaction step is approximately isoergic ($\Delta G = 1$ kcal mol^{-1}). In contrast, the enthalpy barrier is estimated to be only 1 kcal mol^{-1} high, and the peroxyl intermediate is located at −10 kcal mol^{-1} in terms of enthalpy.

Then, **XXII** necessitates to be reduced to **XXIV**. First, a peroxynitrite **XXIII** forms, by coupling of NO to the peroxyl group. There is no barrier to overcome, and the peroxynitrite is lower than **XXII** in enthalpy by −16 kcal mol^{-1} but only by −5 kcal mol^{-1} in terms of free energy. When NO_2 dissociates and leaves the oxyl intermediate **XXIV**, this dissociation limit has the same enthalpy as **XXII** (and there is no barrier for the inverse process), but a further drop of −17 kcal mol^{-1} is estimated in terms of free energy. Here, the same comments of the preceding section on the role of the peroxynitrite intermediate hold, on the basis of the changes observed in going from *H* to *G*. It can also be commented that O_2 addition is again reversible to an extent that depends on [NO]: a low nitrogen monoxide concentration would slow the reduction of **XXII** to the corresponding oxyl radical and make the velocity for O_2 loss from **XXII** competitive.

The likely fate of the oxyl intermediate **XXIV** is to undergo a β fragmentation with formation of a carbonyl group and further cleavage of the endoperoxidic bond. There are convincing indications from our calculations that the partially open-chain intermediate **XXV** shown between brackets in Scheme 2 does not exist. On attempts to define its structure as an energy minimum, the O−O bond spontaneously cleaves, and a second carbonyl forms. Therefore, the two carbonyl groups form concertedly, though in an asynchronous manner (see below). Taking **XXIV** as the reference, the β fragmentation TS is 5 kcal mol^{-1} higher. The open-chain radical intermediate **XVIII** (already encountered in the preceding section) is thus obtained in a very exoergic step ($\Delta G = -61$ kcal mol^{-1}). Its β fragmentation has already been discussed.

The free energy profile is shown in Figure 2a (see also Table 2). The concerted asynchronous transition structure (**XXIV** → **XVIII**) for β fragmentation and subsequent O−O bond cleavage is shown in Figure 2b. Among the major atomic shifts represented in the relevant transition vector, the motions pertinent to the β fragmentation are clearly present, whereas there is no trace of O−O bond cleavage that takes place beyond the TS.

One butenedial isomer has been shown in Scheme 1 and another in Scheme 2. It is however known that 1,4-dicarbonyl compounds easily undergo photoisomerization.[39,40] Butenedial can also undergo further degradation, as it has been shown in either HO•- or O_3-initiated smog chamber experiments on it and its mono- and dimethyl-substituted analogues.[41]

Reaction schemes similar to those proposed by Killus and Whitten for toluene,[35] or by Atkinson, Carter, and Winer for *o*-xylene,[36] and leading to CHO.CHO, CH_3.CO.CHO, CH_3.CO.CO.CH_3 (these two closely related to glyoxal), and CHO.CH=CH.CHO were not explored. The reason is that a localized radical with a bicyclic endoperoxy structure is crucial to both mechanistic proposals. This is the intermediate **XIV**, whose

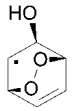

XIV

stability was found modest (+18 vs. −5 kcal mol^{-1} for **XIV** and **XIII**, respectively, relative to the peroxyl adduct **III**) and whose formation implied overcoming a barrier of ca. 25 kcal mol^{-1}, whereas only 14 were required to get **XIII**.[17]

Another sequence of steps can be conceived that originates from **XXII**. A first monomolecular step (in competition with

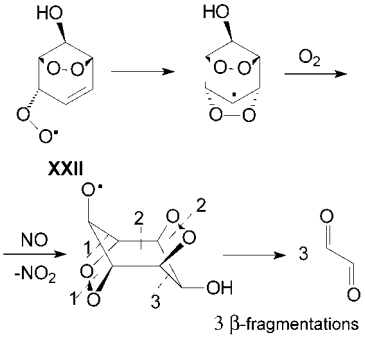

SCHEME 3

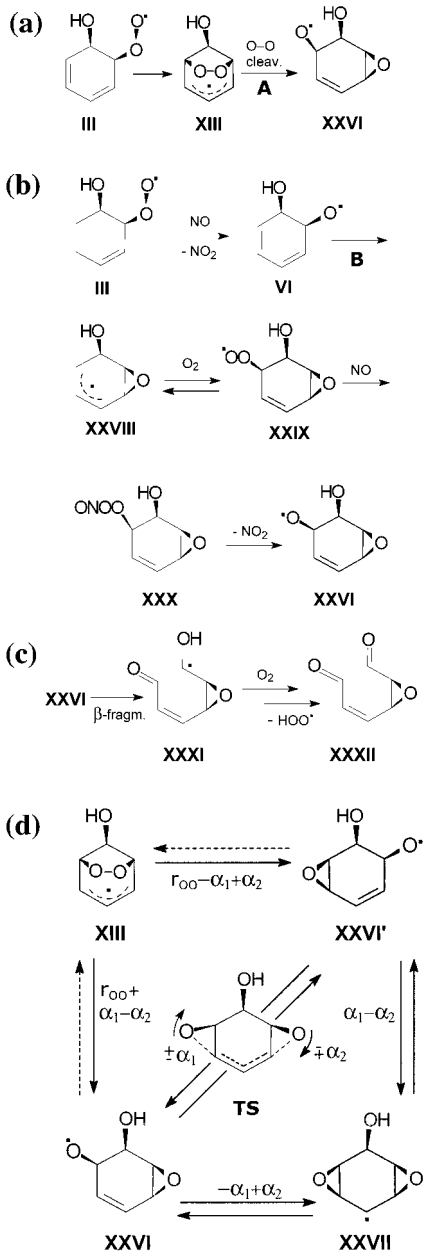

the NO attack of Scheme 2) would generate a tricyclic localized radical by closure of a peroxy bridge. O_2 addition, NO intervention, and a sequence of three β fragmentations would potentially produce glyoxal. However, the first step is associated to an exceedingly high activation electronic energy (39 kcal mol^{-1}), and this pathway cannot be in competition with that of Scheme 2, even in conditions of very low [NO].

3. Epoxy Muconaldehyde from the Early Peroxyl Adduct III. As discussed in a previous paper,[17] two channels branch from the peroxyl intermediate **III** (see Figure 5 in ref 14). The intermediate **XIII** is produced by ring closure (pathway **A**), whereas NO attack onto the terminal oxygen atom of **III** produces **VI**, which is its oxyl analogue (pathway **B**). Once these intermediates are formed, the two reaction channels **A** and **B** lead to a common oxyl epoxy intermediate **XXVI** and finally to the epoxy muconaldehyde **XXXII**. Their details will be examined presently. As can be seen in Scheme 3 parts a and b, pathway **A** does not require O_2 addition to produce an oxyl intermediate (necessary to give ring opening), whereas pathway **B** does, and so it is also characterized by the NO intervention that sets the stage for a subsequent β fragmentation.

TABLE 3: Pathways to the Oxyl-Epoxy Intermediate and Last Steps from It to Epoxy-Muconaldehyde [a]

	ΔE[b]	ΔE[c]	ΔH[d]	ΔG[d]
A. Pathway **A** to the Oxyl-Epoxy Intermediate (and Its Conversion to the Biepoxy Intermediate)[a]				
XIII	0.0	0.0	0.0	0.0
TS **XIII** → **XXVI**	17.7	15.3	14.0	14.0
oxyl-epoxy intermediate **XXVI**	−15.2	−16.4	−16.3	−16.7
TS **XXVI** → **XXVII**	−7.8	−9.5	−10.0	−10.1
bi-epoxy intermediate **XXVII**	−13.1	−13.2	−13.0	−13.4
TS **XXVI** → **XXVI′**	10.8	8.7	7.9	8.0
B. Pathway **B** to the Oxyl-Epoxy Intermediate[a]				
VI	0.0	0.0	0.0	0.0
TS **VI** → **XXVIII**	0.3	0.3	−1.0	−0.1
XXVIII	−9.5	−8.9	−8.9	−8.2
XXVIII + O_2 + NO	0.0	0.0	0.0	0.0
TS **XXVIII** → **XXIX** + NO	2.3	2.5	3.1	13.6
XXIX + NO	−12.9	−7.6	−5.1	6.6
peroxynitrite **XXX**	−34.7	−26.4	−22.1	0.9
XXVI + NO_2	−29.4	−26.4	−24.5	−13.8
C. The Last Steps from the Oxyl-Epoxy Intermediate Toward Epoxy-Muconaldehyde, Common to Pathways **A** and **B**[a]				
oxyl-epoxy intermediate **XXVI**	0.0	0.0	0.0	0.0
β-fragm. TS **XXVI**→ **XXXI**	11.5	10.3	8.6	8.1
XXXI	−3.0	−5.3	−6.3	−10.2
XXXI + O_2	0.0	0.0	0.0	0.0
XXXI−OO•	−28.3	−24.4	−21.5	−10.4
TS **XXXI**-OO → **XXXII** + HOO•	−17.8	−13.9	−14.8	−2.2
XXXII + HOO•	−12.9	−12.8	−12.6	−12.3

[a] For each reaction step: energy, enthalpy, and free energy values (kcal mol^{-1}) relative to each preceding intermediate or intermediate plus reactant. Bold roman numerals make reference to Scheme 4. [b] From DFT(B3LYP)/6-31G(d) energy values obtained at the geometries optimized at the same level. [c] From DFT(B3LYP)/6-311+G(d,p) energy evaluations with correction of spin contamination (at the DFT(B3LYP)/6-31G(d) optimized geometries). [d] From enthalpy or free energy values estimated at 298.15 K. Differential zero-point energy corrections are computed at the DFT(B3LYP)/6-31G(d) level.

In pathway **A**, the cleavage of the O−O bond in **XIII** has a barrier of 14 kcal mol^{-1} and triggers the ring closure of one epoxy ring. The oxyl epoxy intermediate **XXVI** (Scheme 3a) can form this way in a single exoergic step ($\Delta G = -17$ kcal mol^{-1}). This intermediate is closely related to Bartolotti and Edney's[20] epoxidic structure (IV), also labeled as "3,6-1" in that paper, which was estimated to be more stable by −14.0 kcal mol^{-1} than its isomer (III), also labeled as "1,3". This is in turn the methyl-substituted analogue of **XIII** and was found to lie below the analogue of our peroxyl adduct **III**, which was labeled as (II) or "3", by −18.6 kcal mol^{-1}.

As Scheme 3c shows, once the oxyl epoxy intermediate **XXVI** has formed, it can then open via β fragmentation to the radical intermediate **XXXI**, in which the first carbonyl group has formed.[42a] This step is related to a free energy barrier of 8 kcal mol^{-1}.

The open-chain radical **XXXI** is obtained with a free energy gain of 10 kcal mol^{-1} with respect to **XXVI**. An H-abstraction step is necessary for the second carbonyl to form. This can again take place either by simple action of O_2 or via O_2 addition followed by HOO• elimination. The final product is in either case the epoxy muconaldehyde **XXXII**, with a further free energy gain of −12 kcal mol^{-1}. The more convenient way to get also the second carbonyl group is the addition/elimination process, as much as seen in section 1. The relevant free energy profile is shown in Figure 3a (lower curve).

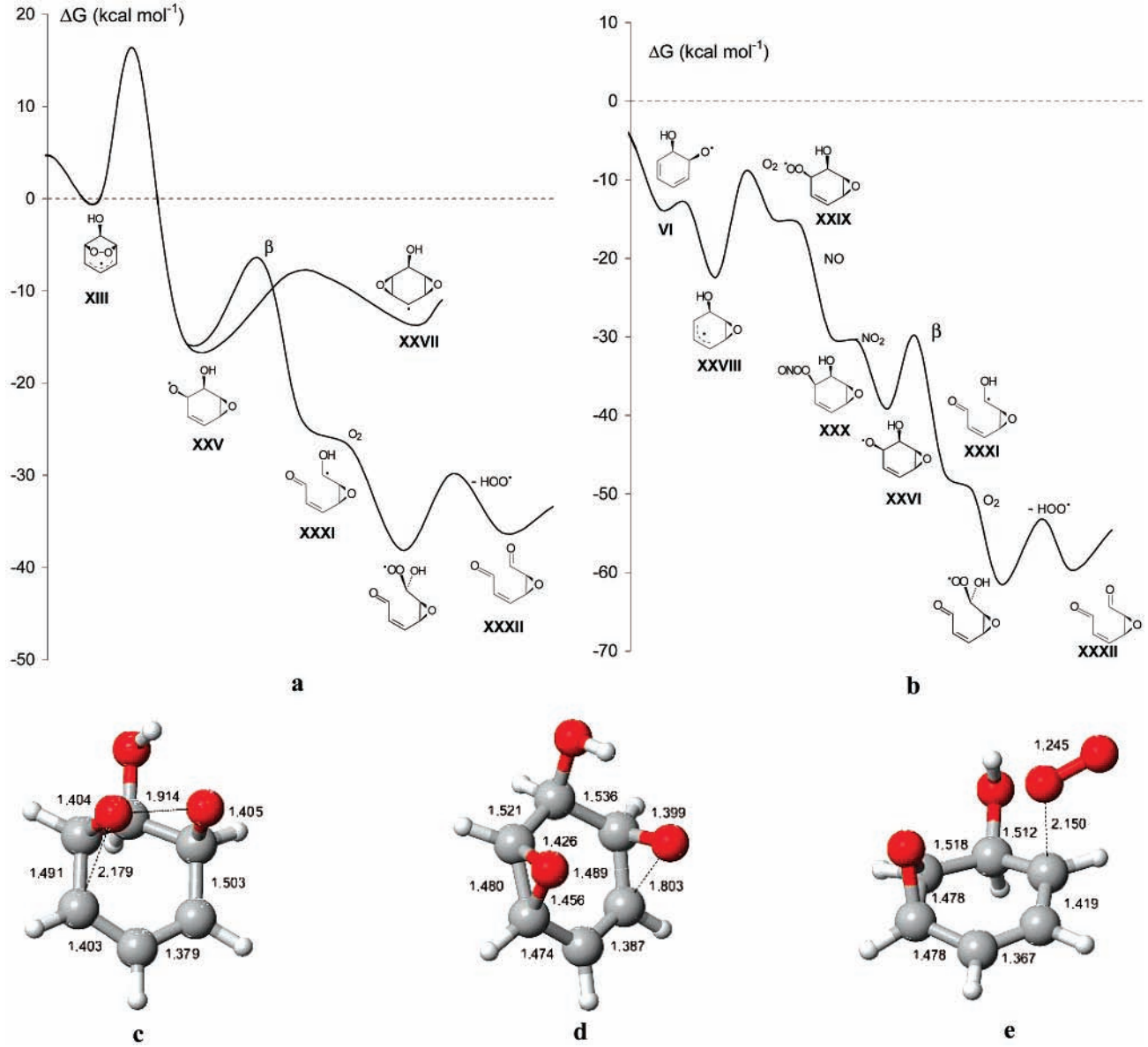

Figure 3. (a) Free energy profile for the formation and interconversion of the epoxy structures. Pathway to epoxy muconaldehyde from the endoperoxy intermediate **XIII**. (b) The free energy profile for the formation of epoxy muconaldehyde from the oxyl intermediate **VI**. (c) The O−O bond cleavage and epoxy ring formation transition structure connecting **XIII** to **XXVI**. Bond lengths are in Å, and angles are in degrees. The interconversion transition structure between epoxy intermediates **XXVI**. Bond lengths are in Å, and angles are in degrees. (d) The O_2 addition to **XXVIII** transition structure. Bond lengths are in Å, and angles are in degrees.

Turning now to pathway **B**, the formation of an epoxide ring in the oxyl compound **VI** is found to take place quite easily. The allyl radical epoxy intermediate **XXVIII** so formed is lower than its precursor **VI**, by −8 kcal mol^{-1} (ΔG). Then reversible O_2 addition to the π-delocalized system takes place, with a low enthalpy barrier ($\Delta H^{\ddagger} = 3$ kcal mol^{-1}) but a more substantial free energy barrier of almost 14 kcal mol^{-1}. The step to the peroxyl adduct **XXIX** is exothermic by −5 kcal mol^{-1} (ΔH) but is endoergic by almost 7 kcal mol^{-1} in terms of free energy. The usual NO addition, with formation of the peroxynitrite **XXX**, takes place without any barrier and is exothermic by −22 kcal mol^{-1} (ΔH) but almost isoergic in terms of ΔG (less than 1 kcal mol^{-1}). In this case, the limit relevant to the oxyl-epoxy intermediate **XXVI** + NO_2 is estimated to have a slightly lower enthalpy than the peroxynitrite **XXX**; hence, NO_2 is described to depart very easily, more so in terms of free energy, as it had been found in other cases ($\Delta G = -15$ kcal mol^{-1} for the peroxinitrite dissociation).

Thus, the intermediate **XXVI** that forms this way is common to the alternative monomolecular pathway **A** that starts off from **XIII** and to the pathway **B** just described. Whichever the channel by which **XXVI** is created, the next step is the six-ring opening via β fragmentation to give **XXXI**, followed by O_2 addition and HOO$^{\bullet}$ elimination, as already seen. The free energy profile for pathway **B** to **XXVI** and then to **XXXII** is shown in Figure 3b.

Let us now consider again the O−O bond cleavage in **XIII**. The oxyl epoxy intermediate can form from **XIII** in two specular ways. The enantiomeric intermediates **XXVI** and **XXVI′** so obtained can interconvert, through a TS in which one epoxy ring is destroyed, whereas the other concertedly forms (center of Scheme 3d). The free energy barrier height for this process is 25 kcal mol^{-1} above **XXVI**. So, the concerted interconversion is not easy, unless **XXVI** is considered as still carrying a significant extra energy coming from its exothermic formation. From each of these intermediates, a biepoxy structure **XXVII**

SCHEME 4

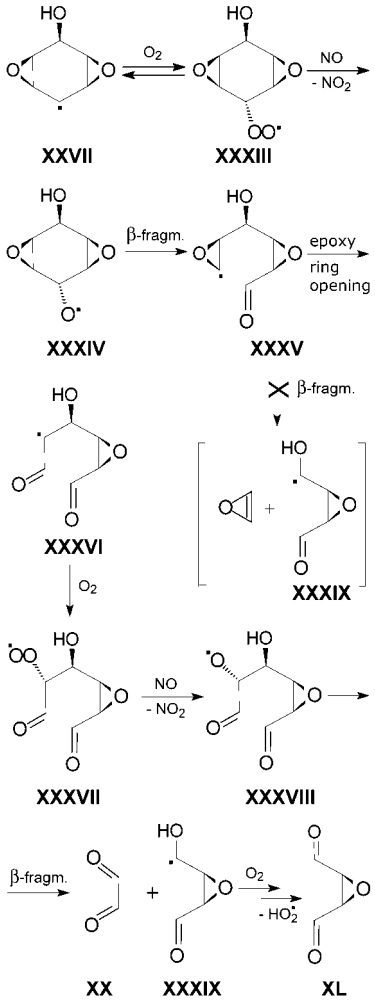

can be reached, by closure of the oxyl group onto the double bond. A localized radical is thus produced. This process is associated to a lower free energy barrier, less than 7 kcal mol^{-1}. The intermediate **XXVII** is higher than the intermediates **XXVI** and **XXVI′** by only 3 kcal mol^{-1}, in terms of free energy. The biepoxy intermediate is in equilibrium with both oxyl epoxy structures, with a ΔG barrier of only 3 kcal mol^{-1}. So, an easier two-step interconversion pathway is available to the system. Inspection of Scheme 3d appears to suggest that the biepoxy structure cannot be reached directly from **XIII**.

The interconversion free energy profile is shown in Figure 3a (upper curve), and the relevant energy data are shown in Table 3a. The transition structure (**XIII** → **XXVI**) for the O−O bond cleavage and concerted epoxidation is shown in Figure 3c. The interconversion transition structure between the enantiomeric epoxy intermediates **XXVI** and **XXVI′** is shown in Figure 3d. The transition structure for O_2 addition to the π-delocalized system of the epoxy intermediate **XXVIII** is shown in Figure 3e.

4. Epoxy Butenedial from the Bicyclic Endo-Peroxy Allyl Radical Intermediate XIII. From the biepoxy intermediate **XXVII** just presented, a convenient series of transformations can produce glyoxal and epoxy butenedial (Scheme 4). Reversible O_2 addition to **XXVII** (to give structure **XXXIII**), followed by NO intervention, generates an oxyl intermediate **XXXIV**, which is prone to undergo a β fragmentation, with formation of a first carbonyl group. The radical **XXXV** so formed could either undergo again a β fragmentation, with formation of oxirene and a precursor of epoxy butenedial **XXXIX** (in brackets), or the opening of one epoxide ring.

TABLE 4: Pathway toward Epoxy-Butenedial[a]

	ΔE[b]	ΔE[c]	ΔH[d]	ΔG[d]
XXVII + O_2 + NO	0.0	0.0	0.0	0.0
XXXIII + NO	−25.9	−22.2	−19.2	−7.8
XXXIV + NO_2	−40.3	−38.7	−36.7	−26.2
XXXIV	0.0	0.0	0.0	0.0
β-fragm. TS **XXXIV** → **XXXV**	18.1	15.5	14.1	12.7
XXXV	11.8	9.9	9.1	6.0
epoxy ring opening TS **XXXV** → **XXXVI**	28.1	24.7	22.6	19.5
XXXVI	−24.5	−27.8	−28.6	−32.1
XXXVI + O_2 + NO	0.0	0.0	0.0	0.0
XXXVII + NO	−18.1	−14.1	−11.8	−0.9
XXXVIII + NO_2	−35.9	−35.3	−34.0	−24.0
XXXVIII	0.0	0.0	0.0	0.0
β-fragm. TS **XXXVIII** → e-**XX** + **XXXIX**	6.8	5.8	4.8	4.4
e-**XX** + **XXXIX**	2.7	−0.4	−2.5	−15.4
XXXIX + O_2	0.0	0.0	0.0	0.0
XL + HOO•	−11.6	−12.0	−12.1	−13.3

[a] For each reaction step: energy, enthalpy, and free energy values (kcal mol^{-1}) relative to each preceding intermediate or intermediate plus reactant. Bold roman numerals make reference to Scheme 4. [b] From DFT(B3LYP)/6-31G(d) energy values obtained at the geometries optimized at the same level. [c] From DFT(B3LYP)/6-311+G(d,p) energy evaluations with correction of spin contamination (at the DFT(B3LYP)/6-31G(d) optimized geometries). [e] From enthalpy or free energy values estimated at 298.15 K. Differential zero-point energy corrections are computed at the DFT(B3LYP)/6-31G(d) level.

The former process is not energetically convenient, and the latter is clearly preferred. By the ring opening, the second carbonyl group forms (structure **XXXVI**). If O_2 adds again to this radical, the usual sequence of events (structures **XXXVII**−**XXXVIII**) opens the way for a further β fragmentation (with formation of glyoxal **XX** and structure **XXXIX**). Finally, production of epoxy butenedial **XL** is possible in an O_2 addition/HOO• elimination phase similar to that presented in section 1. In Figure 4, the ΔG values are reported as if the reaction were proceeding from **XXVI** in Figure 3b. From this and Figure 3a, a relative free energy of −32.3 kcal mol^{-1} is assigned to **XXVII**.

5. Epoxy Butenedial from Butenedial. This section briefly deals with another possibility of getting epoxy aldehydes, the formation of an epoxy ring in the parent aldehydes themselves. The process (exemplified for butenedial, Scheme 5) can be set off by hydroxyl addition to the unsaturated system. Hydrogen abstraction in the adduct **XLI** by dioxygen induces the closure of the epoxy ring. The related energetics make this channel unlikely (Table 5).

6. Glyoxal and Butenedial from the Intermediate XXVIII. Still another pathway branches from that of Scheme 3b (by which the epoxy dialdehydes formed through the intermediacy of **XXVI**). The bifurcation is in correspondence of the epoxy intermediate **XXVIII**, which can undergo reversible O_2 addition to the π-delocalized allyl radical system, not only α to the hydroxyl group, as was shown in Scheme 3b, but also γ to it (Scheme 6).[42b] This different regiochemistry opens a further possibility for the formation of the 1,2- and 1,4-dialdehydes through the usual reaction sequence initiated by the NO intervention and the β fragmentation of the resulting oxyl radical. After the formation of the first carbonyl group, the sequence of steps that follows is quite similar to that shown in Scheme 4 for the biepoxy intermediate. This includes (as sketched in Scheme 6) the opening of the epoxy ring that creates the second carbonyl group, dioxygen addition, and NO intervention. The formation of an oxyl radical triggers a second β fragmentation that produces glyoxal and a precursor of butenedial. A final

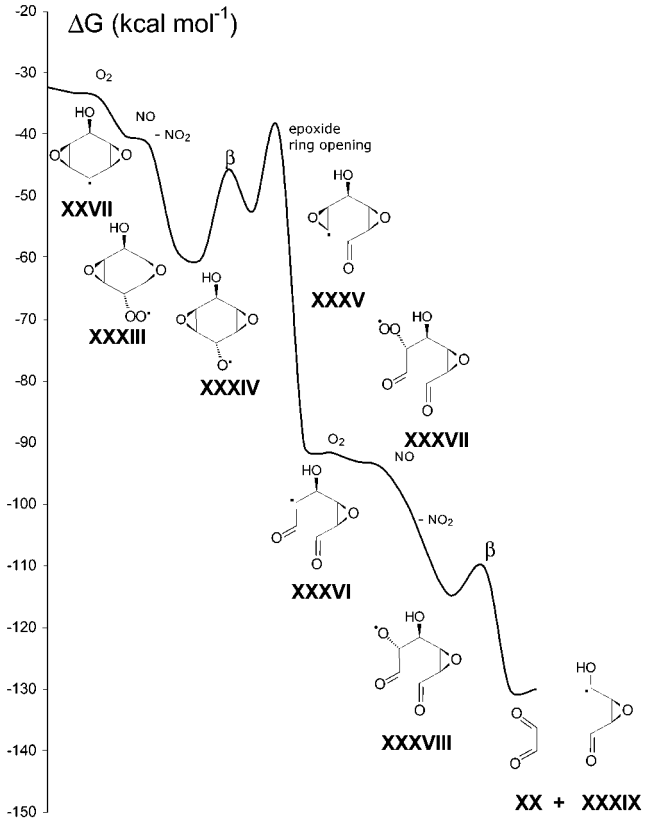

Figure 4. Free energy profile for the formation of epoxy butenedial and glyoxal from the biepoxy intermediate **XXVII**.

SCHEME 5

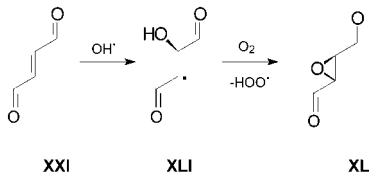

TABLE 5: Formation of Epoxy-Butenedial from the Parent Dialdehyde[a]

	ΔE^b	ΔE^c	ΔH^d	ΔG^d
XXI + HO•	0.0	0.0	0.0	0.0
XLI adduct	−37.1	−33.1	−30.6	−20.3
XLI adduct + O_2	0.0	0.0	0.0	0.0
TS **XLI** + O_2 → **XL** + HOO•	36.5	37.4	34.7	44.5
XL + HOO•	8.0	9.8	9.8	9.4

[a] For each reaction step: energy, enthalpy, and free energy values (kcal mol^{-1}) relative to each preceding intermediate or intermediate plus reactant. Bold roman numerals make reference to Scheme 4. [b] From DFT(B3LYP)/6-31G(d) energy values obtained at the geometries optimized at the same level. [c] From DFT(B3LYP)/6-311+G(d,p) energy evaluations with correction of spin contamination (at the DFT(B3LYP)/6-31G(d) optimized geometries). [d] From enthalpy or free energy values estimated at 298.15 K. Differential zero-point energy corrections are computed at the DFT(B3LYP)/6-31G(d) level.

dioxygen attack onto this intermediate, followed by hydroperoxyl elimination, leads to butenedial.

All of these steps correspond to a free energy cascade that is equivalent to that shown in Figure 4 for the biepoxy intermediate, with the only difference that one epoxy ring is now replaced by a double bond. In view of this fact, only the energetics of the first steps are presented at this point, to allow the consideration of the role of this channel in the Discussion section.

SCHEME 6

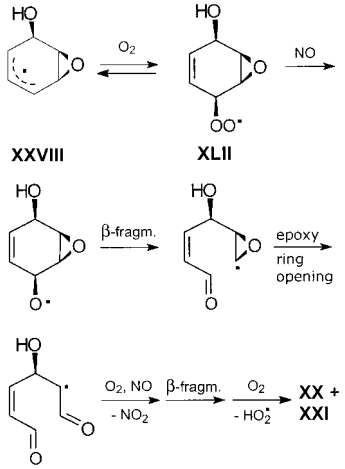

SCHEME 7

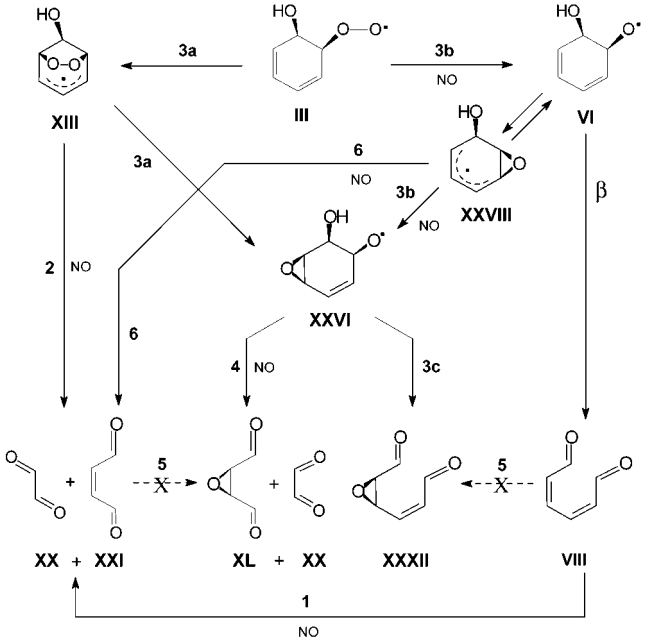

Similarly to the α attack, the γ proceeds with a low enthalpy barrier ($\Delta H^{\ddagger} = 1$ kcal mol^{-1}) but a higher free energy barrier ($\Delta G^{\ddagger} = 11$ kcal mol^{-1}). The step to the peroxyl adduct **XLII** is exothermic by −9 kcal mol^{-1} (ΔH) but is endoergic by 2 kcal mol^{-1} in terms of free energy. The usual NO addition, with formation of a peroxynitrite, takes place by exhibiting the same features already discussed in previous instances. The γ pathway to the aldehydes is thus more favorable, to some extent, than the α, that was shown to bring about the formation of epoxy aldehydes.

Discussion

The viability of the oxidation pathways to 1,2- and 1,4-dialdehydes, and to their epoxy derivatives, will be now examined, with the help of Scheme 7, on the basis of the computational data just presented. In Scheme 7, bold arabic numerals refer to the figures and schemes of the preceding section. Oxidation products can form through channels that either require the intervention of NO or do not. So, the variable concentration of nitrogen oxides could be expected to modulate the relative importance of pathways that imply NO intervention in their energetically more demanding transformation steps vs

pathways that do not. The tropospheric value of [NO_x] ranges approximately from 10^8 to 10^{12} molecules cm^{-3} (ca. 5×10^{-1}–5×10^2 ppb) in going from unpolluted to very polluted areas. It can be higher in some experiments (5−10 ppm)[10,11] or even exceedingly high (of the order of 10^2 ppm) in local situations, as in close proximity of an exhaust source.[45] Therefore, some channels could be in principle thought of as being insignificant or important, depending on the situation. However, if competing NO-dependent and NO-independent processes were converging on the same product, the [NO_x] factor might be ultimately considered as uninfluent on the final result (compare ref 4, p 271). In the following, when estimating how the different pathways compete in the formation of primary products, the steady-state approximation is applied whenever the key steps of a pathway involve reversible formation of one or two intermediates,[46] and [O_2] = 5×10^{18} molecules cm^{-3} is assumed. A stab can be made at the used kinetic constants by inserting in the Eyring equation the computed estimates of the $\Delta G^{\ddagger}$ values for the forward and backward steps connecting the intermediates.

The 2-hydroxy-cyclohexadienyl peroxyl radical **VI** and the bicyclic endo-peroxy allyl-radical intermediate **XIII** intermediates play a central role in the competing and intertwined reaction sequences of the preceding section. Both originate back from the 2-hydroxycyclo-hexadienyl peroxyl radical **III**, an early intermediate in benzene oxidation. NO attack onto the terminal oxygen atom of **III** irreversibly produces **VI**, which is its oxyl analogue (bimolecular process, rate $v_{\mathbf{III-VI}}$). Formation of a peroxy bridge in **III** generates instead the bicyclic intermediate **XIII**, also by an irreversible monomolecular process (rate $v_{\mathbf{III-XIII}}$). Upon inspection of Scheme 7, it is evident that all primary closed-shell products considered in this study can in principle be attained through the intermediacy of **XIII** or **VI** (all-trans compounds alone would appear as exceptions, but only if photoisomerization were disregarded).[39,40] Therefore, it is convenient to define a "channel XIII" as composed by the formation step **III**−**XIII** in pathway **3a**, followed by the continuation of **3a** to give **XXVI**, which is flanked by pathway **2**. Through these two transformations, **XIII** itself is consumed. A "channel VI" can be similarly defined as the **III**−**VI** formation step, followed by the pathways through which **VI** is consumed, namely, **6**, **3b**, and β. In the four situations mentioned above, the ratio $v_{\mathbf{III-XIII}}/v_{\mathbf{III-VI}}$ is ca. 2×10^5 for an unpolluted situation (U), 2×10^1 for a polluted situation (P, the only situation examined in our previous paper[17]), 2×10^{-1} with an NO concentration as that set for some experiments (E), and finally 2×10^{-3} for a peak local value (L).

The relative importance of the two pathways that contribute to channel XIII, **2** and **3a** (Scheme 7, left), as that of the pathways that contribute to channel VI, **6**, **3b**, and β (Scheme 7, right), can also be estimated. The result will depend on NO concentration. Pathways **2**, **3b**, and **6** involve the reversible formation of O_2 adducts, whereas another equilibrium is present beetwen intermediate **VI** and **XXVIII**. The relevant rate ratios (see the Supporting Information for the full equations) are as follows, depending on the four situations defined above. Channel XIII: $v_{\mathbf{3a}}/v_{\mathbf{2}} \approx 2 \times 10^8$ (U), 2×10^4 (P), 2×10^2 (E), and 2 (L). Channel VI: $v_{\beta}/v_{\mathbf{6}} \approx 2 \times 10^{11}$ (U), 2×10^7 (P), 2×10^5 (E), and 2×10^5 (L), whereas $v_{\beta}/v_{\mathbf{3b}} \approx 3 \times 10^{14}$ (U), 3×10^{10} (P), 3×10^8 (E), and finally 2×10^8 (L).

Once the intermediate **XXVI** is formed, both epoxy dialdehydes originate from it, by distinct pathways, **3c** and **4**. On the one hand, **XXXII** is obtained by an irreversible β fragmentation (**3c**). On the other hand, **XL** can form through pathway **4**, which begins with the reversible formation of the biepoxide **XXVII**, followed by a reversible O_2 addition. The following values are obtained for the relevant rate ratio, depending on [NO]: $v_{\mathbf{3c}}/v_{\mathbf{4}} \approx 5 \times 10^8$ (U), 5×10^4 (P), 5×10^2 (E), and 5×10^1 (L).

TABLE 6: Relative Flows[a] along the Channels that Originate from III and Lead to the Products

situation:[b] [NO] =	unpolluted 5 ppt	polluted 50 ppb	expt 5 ppm	local peak 500 ppm
XIII	∼1	∼1	2×10^{-1}	2×10^{-3}
VI	$<10^{-5}$	4×10^{-2}	8×10^{-1}	∼1
		Channel XIII		
XXVI	∼1	∼1	2×10^{-1}	2×10^{-3}
XX + **XXI**[c]	$<10^{-5}$	5×10^{-5}	1×10^{-3}	7×10^{-4}
		Channel VI		
XXVI	$<10^{-5}$	$<10^{-5}$	$<10^{-5}$	$<10^{-5}$
VIII	$<10^{-5}$	4×10^{-2}	8×10^{-1}	∼1
XX + **XXI**[c]	$<10^{-5}$	$<10^{-5}$	$<10^{-5}$	$<10^{-5}$
XX + **XXI**[d]	$<10^{-5}$	$<4 \times 10^{-2}$	$<8 \times 10^{-1}$	<1
		From **XXVI**		
XXXII	∼1	∼1	2×10^{-1}	2×10^{-3}
XX + **XL**	$<10^{-5}$	2×10^{-5}	4×10^{-4}	3×10^{-5}

[a] Yields of the intermediates and products, having set to 1 the availability of the intermediate **III**. [b] See text, and the Supporting Information for [NO] values in different units. [c] As primary products (see text). [d] As secondary products, from **VIII** (see text).

Table 6 contains information on the flows along the various channels open to the early intermediate **III**, for the four NO concentrations considered above, i.e., the yields of the various intermediates and products, if the availability of the intermediate **III** is set to 1. An obvious caution is that the information has to be seen as only qualitative, because of the different approximations used, as the intrinsic limitations of the computed free energy values, and the choice made once and for all for the concentration of O_2 used in the calculations. Though very approximate, nevertheless these estimates suggest some trends. (1) The relative importance of **VI** and **XIII**, hence, of the channels that originate from them, changes drastically as [NO] rises. (2) **XXVI** irreversibly forms via channel **XIII** in every situation, whereas the contribution to its formation by channel **VI** is negligible. (3) From **XXVI**, only epoxy muconaldehyde can be an important product. (4) Glyoxal and butenedial are minor *primary* products. (5) The formation of **VIII** via the pathway β is strongly dependent on [NO]. (6) When [NO] is high, a more important source of glyoxal and butenedial (as *secondary* products) could be the further oxidation of **VIII** itself (pathway **1**).

The closed shell stable intermediate **VIII** has a chance to get in thermal equilibrium with the surrounding gas before encountering hydroxyl, and so the HO$^{\bullet}$ + **VIII** system can be supposed, when reacting, to carry none of the extra energy coming from the free energy cascade of Figure 5 in ref 17. It has thus to overcome a barrier of more than 6 kcal mol^{-1}. With a hydroxyl concentration of only 1.7×10^{-15} M (i.e., ca. 10^6 molecules cm^{-3}, an average tropospheric value), we see that the formation of **XX** and **XXI** through channel VI has to slow considerably. Thus, a relatively smaller amount of dialdehydes can be expected to form rather early via pathway **2** and **6**, whereas the greater part will come from pathway **1**, but with some delay.

These comments can be compared to the findings of Yu, Jeffries, and Sexton.[10] Glyoxal (and methylglyoxal) exhibited two peaks in their concentration/time plots (ref 10, Figure 5). Butenedial had indeed a single peak, but the methylated derivative 4-oxo-2-pentenal showed two again. A rather early

single peak was interpreted as a sign of quick reaction after formation as a primary product or, as an alternative, as a product from early, short-lived intermediates. The double maxima of glyoxal and methylglyoxal indicated them as both primary and secondary products, possibly forming from both early and subsequent reaction intermediates.

Finally, we can remark that hydroperoxyl formation has been considered only in the concluding steps of the formation of both dialdehydes and dialdehyde epoxides. So, the "prompt" ($t <$ 50 ms) formation of $HOO^{\bullet}$, which was experimentally detected by Zetzsch and co-workers,[43] cannot be associated to them. It could more likely related to the easy and irreversible phenol formation discussed in a preceding paper.[16]

Conclusions

In this theoretical study, the viability of some benzene oxidation pathways, which lead to the formation of 1,2- and 1,4-dialdehydes and to their epoxy derivatives, is discussed. Both the [3.2.1] bicyclic endo-peroxy allyl radical **XIII** and the 2-hydroxycyclo-hexadienyl oxyl radical **VI** (which are irreversibly formed rather early in the oxidation of benzene) play key roles in the formation of dialdehydes and dialdehyde epoxides. Their relative importance is dependent on the concentration of NO, which is involved in the formation of **VI** but not of **XIII**. Of the pathways that stem from **VI** and **XIII**, some involve reversible initial steps and some do not. By taking into account all of these processes, four scenarios are depicted. (1) In unpolluted tropospheric conditions, the largely prevailing channel passes through **XIII**, and from it, epoxy muconaldehyde is essentially the only primary product. (2) In polluted conditions, this situation is slightly modified, in that up to 4% formation of **VI** can be predicted from our estimates. This implies that a minor amount of muconaldehyde can form along with the major product epoxy muconaldehyde. Glyoxal and butenedial can form in turn from its oxidation as secondary products. (3) The [NO] can be higher in some experiments: by setting it to 5 ppm, **VI** and **XIII** would form in a 4:1 ratio. Now it can be reckoned that muconaldehyde has become the major product, and its formation (or that of glyoxal and butenedial as secondary products) is significantly more important than the formation of epoxy muconaldehyde. (4) As a last scenario, an exceedingly high [NO] can be hypothesized for a local situation, as in close proximity of an exhaust source. Now, **XIII** would form sluggishly relative to **VI** (approximately by 3 orders of magnitude). A rising NO concentration would bolster formation of muconaldehyde (and then of glyoxal and butenedial), whereas the epoxy dialdehydes would be very minor products.

Acknowledgment. Financial support was provided in part by the Italian MURST through the "Cofinanziamento di Programmi di Ricerca di Rilevante Interesse Nazionale", within the project "Chimica in Fase Gassosa di Specie Reattive Neutre e Cariche". This project was also supported in part by the Italian CNR, within the project "Modellistica Computazionale di Sistemi Molecolari Complessi". The figures of the transition structures were drawn with MolMol 2.4.[44]

Supporting Information Available: A listing of geometries, total energies, enthalpies, and free energies at various computational levels. The equations used in the Discussion section. This material is available free of charge via the Internet at http://pubs.acs.org

References and Notes

(1) Becker, K. H.; Barnes, I.; Ruppert, L.; Wiesen, P. Free radicals in the atmosphere: the motor of tropospheric oxidation processes. In *Free Radicals in Biology and Environment*; Minisci, F., Ed.; Kluwer Academic Publishers: Norwell, MA, 1997; Chapter 27, pp 365−385 and references therein.

(2) Güsten, H. Degradation of atmospheric pollutants by tropospheric free radical reactions. In *Free Radicals in Biology and Environment*; Minisci, F., Ed.; Kluwer Academic Publishers: Norwell, MA, 1997; Chapter 28, pp 387−408.

(3) Grosjean, D. *Science Total Environ.* **1991**, *100*, 367−414.

(4) Atkinson, R. Reactions of Oxygen Species in the Atmosphere. In *Active Oxygen in Chemistry*; Valentine, J. S., Foote, C. S., Greenberg, A., Liebman, J. F., Eds.; Blackie Academic and Professional, Chapmann & Hall: New York, 1995; Ch. 7.

(5) Knispel, R.; Koch, R.; Siese, M.; Zetzsch, C. *Ber. Bunsen-Ges. Phys. Chem.* **1990**, *94*, 1375−1379. Reported rate constants for the reaction of hydroxycyclohexadienyl with NO_2, NO, and O_2 are ca. 3×10^{-11} cm^3 $molecule^{-1}$ s^{-1}, less than 3×10^{-14} cm^3 $molecule^{-1}s^{-1}$, and ca. 2×10^{-16} cm^3 $molecule^{-1}$ s^{-1}, respectively. See also: Zetzsch, C.; Koch, R.; Bohn, B.; Knispel, R.; Siese, M.; Witte, F. *Transp. Chem. Transform. Pollut. Troposphere*; Le Bras, G., Ed.; Springer: Berlin, 1997; Vol. 3, pp 347−256.

(6) Wayne, R. P. *Chemistry of Atmospheres*; Clarendon Press: Oxford, 1996; pp 252−263.

(7) Atkinson, R. *J. Phys. Chem. Ref. Data* **1994**, Monograph No. 2, 1−216; **1989**, Monograph No. 1, 1−246.

(8) Seuwen, R.; Warneck, P. *Int. J. Chem. Kinet.* **1996**, *28*, 315−332.

(9) Dumdei, B. E.; O'Brien R. J. *Nature* **1984**, *311*, 248−250.

(10) Yu, J.; Jeffries, H. E.; Sexton, K. G. *Atmos. Environ.* **1997**, *31*, 2261−2280.

(11) Yu, J.; Jeffries, H. E. *Atmos. Environ.* **1997**, *31*, 2281−2287.

(12) Klotz, B.; Barnes, I.; Becker, K. H.; Golding, B. T. *J. Chem. Soc., Faraday Trans.* **1997**, *93*, 1507−1516.

(13) Shepson, P. B.; Edney, E. O.; Corse, E. W. *J. Phys. Chem.* **1984**, *88*, 4122−4126.

(14) Sorensen, S.; Klotz, B.; Barnes, I.; Becker, K. H. *Proc. NOSA/NORSAC Symp.* **1996**, 27−29.

(15) Dibble, T. S. *J. Am. Chem. Soc.* **2001**, *123*, 4228−4234.

(16) Ghigo, G.; Tonachini, G. *J. Am. Chem. Soc.* **1998**, *120*, 6753−6757.

(17) Ghigo, G.; Tonachini, G. *J. Am. Chem. Soc.* **1999**, *121*, 8366−8372.

(18) Greenberg, A. Exploration of Selected Pathways for Metabolic Oxidative Ring Opening of Benzene Based on Estimates of Molecular Energetics. In *Active Oxygen in Biochemistry*; Valentine, J. S., Foote, C. S., Greenberg, A., Liebman, J. F., Eds.; Blackie Academic and Professional, Chapmann & Hall: New York, 1995; pp 413−417, Ch. 8.

(19) Bleasdale, C.; Kennedy, G.; MacGregor, J. O.; Nieschalk, J.; Pearce, K.; Watson, W. P.; Golding, B. T. Chemistry of muconaldehydes of possible relevance to the toxicology of benzene. In *Environmental Health Perspectives Suppl.*; (6, *Benzene Toxicity, Carcinogenesis, and Epidemiology*); U.S. Department of Health and Human Services: Washington, DC, 1996; Vol. 104, pp 1201−1209.

(20) Bartolotti, L. J.; Edney, O. E. *Chem. Phys. Lett.* **1995**, *245*, 119−122.

(21) Andino, J. M.; Smith, J. N.; Flagan, R. C.; Goddard, W. A., III.; Seinfeld, J. H. *J. Phys. Chem.* **1996**, *100*, 10967−10980.

(22) Lay, T. H.; Bozzelli, J. W.; Seinfeld, J. H. *J. Phys. Chem.* **1996**, *100*, 6543−6554.

(23) Benson, S. W. *Thermochemical Kinetics*; Wiley-Interscience: New York, 1976.

(24) Uc, V. H.; Garcìa-Cruz, I.; Hernàndez-Laguna, A.; Vivier-Bunge, A. *J. Phys. Chem. A* **2000**, *104*, 7847−7855.

(25) Garcìa-Cruz, I.; Castro, M.; Vivier-Bunge, A. *J. Comput. Chem.* **2000**, *21*, 716−730.

(26) A large part of the results discussed in this paper were collected within the "Tesi di Laurea" work by F.M. (University of Torino, july 2000). Some preliminary results have been reported by G.T. at the joint workshop of the Deutsche Bundesstiftung Umwelt, Società Chimica Italiana, and Gesellschaft Deutscher Chemiker on *Atmospheric Diagnostics and Tropospheric Chemistry*, held in St. Marienthal, Germany, June, 2000.

(27) Pople, J. A.; Gill, P. M. W.; Johnson, B. G. *Chem. Phys. Lett.* **1992**, *199*, 557−560. Schlegel, H. B. In *Computational Theoretical Organic Chemistry*; Csizsmadia, I. G., Daudel, Eds.; Reidel Publ. Co.: Dordrecht, The Netherlands, 1981; p.129−159. Schlegel, H. B. *J. Chem. Phys.* **1982**, *77*, 3676−3681. Schlegel, H. B.; Binkley, J. S.; Pople, J. A. *J. Chem. Phys.* **1984**, *80*, 1976−1981. Schlegel, H. B. *J. Comput. Chem.* **1982**, *3*, 214−218.

(28) (a) Parr, R. G.; Yang, W. *Density Functional Theory of Atoms and Molecules*; Oxford University Press: New York, 1989; Chapter 3. (b) Becke, A. D. *Phys. Rev. A* **1988**, *38*, 3098−3100. (c) Becke, A. D. *ACS Symp. Ser.* **1989**, *394*, 165. (d) Becke, A. D. *J. Chem. Phys.* **1993**, *98*, 5648−5652. (e) Pople, J. A.; Gill, P. M. W.; Johnson, B. G. *Chem. Phys. Lett.* **1992**, *199*, 557−560. (f) Lee, C.; Yang, W.; Parr, R. G. *Phys. Rev. B* **1988**,

37, 785−789. (g) Jensen, F. *Introduction to Computational Chemistry*; John Wiley: New York, 1999.

(29) This theory level was tested on a model reaction and compared with more expensive ab initio methods: Ghigo, G.; Tonachini, G. *J. Chem. Phys.* **1999**, *109*, 7298−7304. It appeared to be a rather good compromise between reliability and feasibility in studying the degradation of aromatics and was then used in refs 16 and 17. This approach is based on a popular hybrid exchange-correlation functional, made up by the three term exchange functional propounded by Becke, B3 (ref 28b−d), and by the correlation functional of Lee, Yang, and Parr, LYP (ref 28f). It has encountered widespread success because of its rather satisfactory performances. See for instance ref 28g, p 189.

(30) (a) Hehre, W. J.; Ditchfield, R.; Pople, J. A. *J. Chem. Phys.* **1972**, *56*, 2257−2261. Hariharan, P. C.; Pople, J. A. *Theor. Chim. Acta* **1973**, *28*, 213−222. (b) Diffuse functions: Clark, T.; Chandrasekhar, J.; Schleyer, P. v. R. *J. Comput. Chem.* **1983**, *4*, 294−301. (c) 6-311+G(d,p): Frisch, M. J.; Pople, J. A.; Binkley, J. S. *J. Chem. Phys.* **1984**, *80*, 3265−3269.

(31) Yamanaka, S.; Kawakami, T.; Nagao, K.; Yamaguchi, K. *Chem. Phys. Lett.* **1994**, *231*, 25−33. Yamaguchi, K.; Jensen, F.; Dorigo, A.; Houk, K. N. *Chem. Phys. Lett.* **1988**, *149*, 537−542. See also: Baker, J.; Scheiner, A.; Andzelm, J. *Chem. Phys. Lett.* **1993**, *216*, 380−388.

(32) For discussions concerning the effect of spin projection on the performances of DFT methods, see: Wittbrodt, J. M.; Schlegel, H. B. *J. Chem. Phys.* **1996**, *105*, 6574−6577 (in which some drawbacks of the projection procedures are discussed, that can suggest not to use them). Goldstein, E.; Beno, B.; Houk, K. N. *J. Am. Chem. Soc.* **1996**, *118*, 6036−6043.

(33) Reaction enthalpies and entropies were computed as outlined, for instance, in: Foresman, J. B.; Frisch, Æ. *Exploring Chemistry with Electronic Structure Methods*; Gaussian, Inc.: Pittsburgh, PA, 1996, pp 166−168. McQuarrie, D. A. *Statistical Thermodynamics*; Harper and Row: New York, 1973; Chapter 8.

(34) Frisch, M. J.; Trucks, G. W.; Schlegel, H. B.; Scuseria, G. E.; Robb, M. A.; Cheeseman, J. R.; Zakrzewski, V. G.; Montgomery, J. A., Jr.; Stratmann, R. E.; Burant, J. C.; Dapprich, S.; Millam, J. M.; Daniels, A. D.; Kudin, K. N.; Strain, M. C.; Farkas, O.; Tomasi, J.; Barone, V.; Cossi, M.; Cammi, R.; Mennucci, B.; Pomelli, C.; Adamo, C.; Clifford, S.; Ochterski, J.; Petersson, G. A.; Ayala, P. Y.; Cui, Q.; Morokuma, K.; Malick, D. K.; Rabuck, A. D.; Raghavachari, K.; Foresman, J. B.; Cioslowski, J.; Ortiz, J. V.; Stefanov, B. B.; Liu, G.; Liashenko, A.; Piskorz, P.; Komaromi, I.; Gomperts, R.; Martin, R. L.; Fox, D. J.; Keith, T.; Al-Laham, M. A.; Peng, C. Y.; Nanayakkara, A.; Gonzalez, C.; Challacombe, M.; Gill, P. M. W.; Johnson, B. G.; Chen, W.; Wong, M. W.; Andres, J. L.; Head-Gordon, M.; Replogle, E. S.; Pople, J. A. *Gaussian 98*, revision A.6; Gaussian, Inc.: Pittsburgh, PA, 1998.

(35) Killus, J. P.; Whitten, G. Z. *Atmos. Environ.* **1983**, *17*, 1597−1598.

(36) Atkinson, R.; Carter, W. P. L.; Winer, A. M. *J. Phys. Chem.* **1983**, *97*, 1605−1610.

(37) Klotz, B.; Bierbach, A.; Barnes, I.; Becker, K. H. *Environ. Sci. Technol.* **1995**, *29*, 2322−2332.

(38) Darnall, K. R.; Atkinson, R.; Pitts, J. N., Jr. *J. Phys. Chem.* **1979**, *83*, 1943−1946.

(39) Bierbach, A.; Barnes, I.; Becker, K. H.; Wiesen, E. *Environ. Sci. Technol.* **1994**, *29*, 715−729.

(40) Tuazon, E. C.; Atkinson, R.; Carter, W. P. L. *Environ. Sci. Technol.* **1985**, *19*, 265−269.

(41) Liu, X.; Jeffries, H. E.; Sexton, K. G. *Environ. Sci. Technol.* **1999**, *33*, 4212−4220.

(42) (a) When **XXVI** is generated by O_2 addition to **XXVIII**, to give **XXIX** and **XXX** (section 4 and Scheme 4), the addition can take place also on the opposite face of the six-ring (with respect to the epoxy oxygen). A trans diastereomer of **XXVI** would thus be formed that could also originate, in turn, a trans biepoxy intermediate diastereomer of **XXVII**. Given that these different possibilities would lead anyway to the same intermediate **XXXI**, this line of investigation was not pursued any further. (b) A similar argument holds for the O_2 addition to **XXVIII** discussed in section 6 (Scheme 6).

(43) Siese, M.; Koch, R.; Fittschen, F.; Zetzsch, C. Cycling of OH in the Reaction Systems Toluene/O_2/NO and acetylene/O_2 and the addition of OH to Isoprene. In *Transport and Transformation of Pollutants in the Troposphere Proceedings of EUROTRAC Symposium 94*; Borrel, P. M., Borrel, P., Cvitas, T., Seiler, W., Eds.; SPB Academic Publishing bv.: The Hague, The Netherlands, 1994; pp 115−119.

(44) MolMol 2.4. A graphic program developed by the Institut für Molekular-Biologie und Biophysik, EHT Zurich Spectrospin AG, Faellenden, Switzerland. Koradi, R.; Billeter, M.; Wüthrich, K. *J. Mol. Graphics* **1996**, *14*, 51−55.

(45) Restelli, G.; Zanderighi, G. *Chimica dell'Atmosfera e dell'Inquinamento Atmosferico*; Edizioni Unicopli: Milano, Italy, 2001; p 98.

(46) Carpenter, B. K. *Determination of Organic Reaction Mechanisms*; Wiley-Interscience: New York, 1984; Chapter 4.